

# YALE PEABODY MUSEUM

P.O. BOX 208118 | NEW HAVEN CT 06520-8118 USA | PEABODY.YALE. EDU

## JOURNAL OF MARINE RESEARCH

The *Journal of Marine Research*, one of the oldest journals in American marine science, published important peer-reviewed original research on a broad array of topics in physical, biological, and chemical oceanography vital to the academic oceanographic community in the long and rich tradition of the Sears Foundation for Marine Research at Yale University.

An archive of all issues from 1937 to 2021 (Volume 1–79) are available through EliScholar, a digital platform for scholarly publishing provided by Yale University Library at <https://elischolar.library.yale.edu/>.

Requests for permission to clear rights for use of this content should be directed to the authors, their estates, or other representatives. The *Journal of Marine Research* has no contact information beyond the affiliations listed in the published articles. We ask that you provide attribution to the *Journal of Marine Research*.

Yale University provides access to these materials for educational and research purposes only. Copyright or other proprietary rights to content contained in this document may be held by individuals or entities other than, or in addition to, Yale University. You are solely responsible for determining the ownership of the copyright, and for obtaining permission for your intended use. Yale University makes no warranty that your distribution, reproduction, or other use of these materials will not infringe the rights of third parties.



This work is licensed under a Creative Commons Attribution-NonCommercial-ShareAlike 4.0 International License.  
<https://creativecommons.org/licenses/by-nc-sa/4.0/>



# **New observations of the intermediate depth circulation in the tropical Atlantic**

by **Claudia Schmid<sup>1,2</sup>**, **Robert L. Molinari<sup>2</sup>** and **Silvia L. Garzoli<sup>2</sup>**

## **ABSTRACT**

The intermediate depth (around 1000 m) circulation in the interior tropical Atlantic has been described as several narrow flow bands. Due to a lack of data, these currents have previously been poorly resolved in space and time. Recent observations, obtained during the mid-1997 *Seward Johnson* cruise and from PALACE floats which cover the period Summer 1997 to Spring 2000, allow a more detailed description of the intermediate depth circulation in the tropical Atlantic. The PALACE trajectories display several well defined currents between the equator and 4N at 800 to 1100 m. Two regimes separated by the eastern edge of the Mid-Atlantic Ridge seem to exist at these latitudes. Velocities in the eastern regime are lower than in the western regime and at some latitudes, the zonal flow in the two regimes is going in opposite directions. Farther south, between 4S and 2S, westward velocities of the central South Equatorial Current dominate the circulation. The flow north of 4N and south of 4S is governed by up to several month-long periods of eastward or westward flow, with only weak preferences for either direction. The southern region is characterized by the (meandering) transition between the central South Equatorial Current and the South Equatorial Countercurrent. It has been proposed earlier that these two currents do not extend eastward beyond about 10W, and that the intermediate water follows a cyclonic path east of 10W between about 5S and 25S. This could be interpreted as an intermediate expression of the Angola Gyre. Such a circulation is not found in the present data set. It is also noted that no significant cross-equatorial flow is found in the PALACE data.

## **1. Introduction**

Knowledge of the main water mass pathways through the tropical Atlantic is needed to fully understand the meridional overturning cell. The overturning cell consists of North Atlantic Deep Water (NADW) flowing south, and the water masses above and below the NADW flowing north. The focus of this study will be on the characteristics of tropical circulation at intermediate depth (800 to 1100 dbar) which is part of the northward branch of the overturning cell.

The large-scale circulation in the tropical Atlantic has recently been reviewed by Stramma and Schott (1999). They presented a schematic flow diagram for the currents in a

1. Cooperative Institute for Marine and Atmospheric Studies, University of Miami, Miami, Florida, 33149, U.S.A.

2. NOAA/Atlantic Oceanographic and Meteorological Laboratory, 4301 Rickenbacker Causeway, Miami, Florida, 33149, U.S.A. *email: schmid@aoml.noaa.gov*

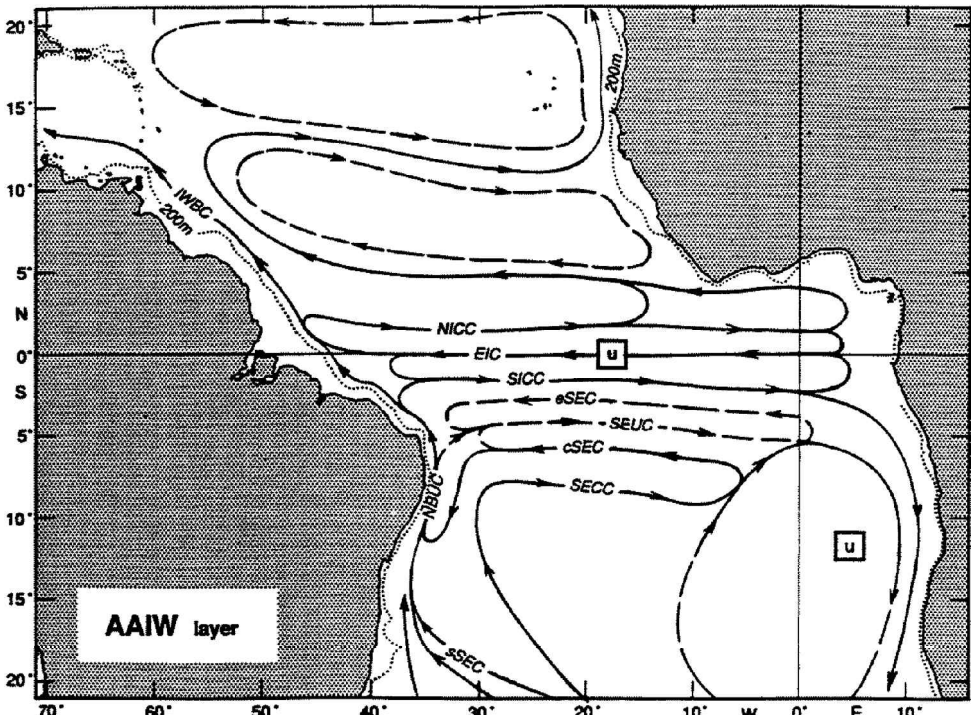


Figure 1. Schematic flow diagram for 500 to 1200 m depth. Reprinted from *Deep-Sea Research II*, 46, Stramma and Schott (1999), pages 279–303, Copyright 2000, with permission from Elsevier Science. The abbreviations are: Northern Intermediate Countercurrent (NICC), Equatorial Intermediate Current (EIC), Southern Intermediate Countercurrent (SICC), South Equatorial Current (SEC), equatorial SEC (eSEC), central SEC (cSEC), southern SEC (sSEC), South Equatorial Undercurrent (SEUC), South Equatorial Countercurrent (SECC), North Brazil Undercurrent (NBUC), and Intermediate Western Boundary Current (IWBC).

column extending from 500 to 1200 m (Fig. 1). The diagram shows the zonal flow bands of the tropical Atlantic, the boundary currents, and a cyclonic gyre south of 5S in the eastern South Atlantic. The major zonal currents south of the equator are the eastward South Equatorial Countercurrent (SECC, near 8S), the westward central South Equatorial Current (cSEC, near 6S) and the eastward Southern Intermediate Countercurrent (SICC, around 2S). Additionally, two weaker currents might exist: a deep extension of the South Equatorial Undercurrent (SEUC, near 4S) and the equatorial South Equatorial Current (eSEC, near 3S).

The pattern of alternating currents continues at and north of the equator. The schematic shows the westward Equatorial Intermediate Current (EIC) along the equator, and the eastward Northern Intermediate Countercurrent (NICC) at about 2N and a westward current near 5N. Water parcels entering the western tropics from the south can either

continue north along the boundary or undergo considerable zonal translations before exiting along either boundary.

Geostrophic sections, when plotted as a function of time and longitude, show that the tropical Atlantic currents at intermediate depths can vary considerably in width and location (Fig. 2). The eastward flow undulating between 9.5S and 3S is associated with the SECC of Figure 1, and the westward flow between 7S and 2S with the cSEC.

Three water masses have been described in the 500 to 1500 dbar range, the Antarctic Intermediate Water (AAIW), the upper Circumpolar Deep Water (uCDW) and the upper North Atlantic Deep Water (uNADW). The AAIW, characterized by a salinity minimum, is observed between 700 and 900 dbar in the tropical Atlantic. Suga and Talley (1995), using hydrographic data, argue that AAIW enters the tropics near the western boundary of the South Atlantic. Portions of AAIW are then advected eastward in two latitude bands as indicated by weak tongues of low salinity at intermediate depths ( $27.3 \text{ kg m}^{-3}$  in  $\sigma_\theta$ ). One tongue is located between 3S and 4S, the latitude of the SICC, and the other between 1N and 2N, the latitude of the NICC.

The southern hemisphere uCDW is also advected to the tropical Atlantic. It is characterized by a temperature minimum located between the AAIW and the uNADW and centered at about 1000 dbar. Earlier studies suggest that the uCDW does not penetrate northward across the equator (Reid, 1989). Other authors, e.g. Tsuchiya *et al.* (1994), considered the temperature minimum as the lower boundary of the AAIW and not as a distinct water mass. The temperature maximum of the uNADW can be found near 1300 dbar.

Circulation patterns in the tropical Atlantic have also been derived from direct current observations with profiling floats (Molinari *et al.*, 1999). They used a subset of the data considered herein and identified three zonal currents in the float trajectories: the EIC, the NICC and a westward current around 4N. The meridional scale of these currents is on the order of  $2^\circ$ . In contrast, Richardson and Schmitz (1993) reporting on the trajectories of six subsurface floats observed only eastward flow between 5S and 6N. The authors stated: ‘Of course, regions of westward flow could be embedded in the eastward current, [ . . . ], and a few are seen.’ Schott *et al.* (1998) found the NICC between 1N and 3N at 44W and 35W but with some temporal variability at these locations (the velocity range between 800 and 1000 dbar was  $10 \text{ cm s}^{-1}$  to  $30 \text{ cm s}^{-1}$  at 44W, and was approximately  $10 \text{ cm s}^{-1}$  at 35W).

In this paper, Lagrangian and Eulerian current measurements, as well as hydrographic observations, will be used to describe the structure and temporal variability of the intermediate depth flow field of the tropical Atlantic. The remainder of this study is structured as follows: A description of the data (Section 2) is followed by a discussion of the water masses observed in the region (Section 3). Afterward, the conditions at float deployment are summarized and the ensuing float trajectories are described (Section 4). These observations will be discussed in the context of earlier studies (Section 5).

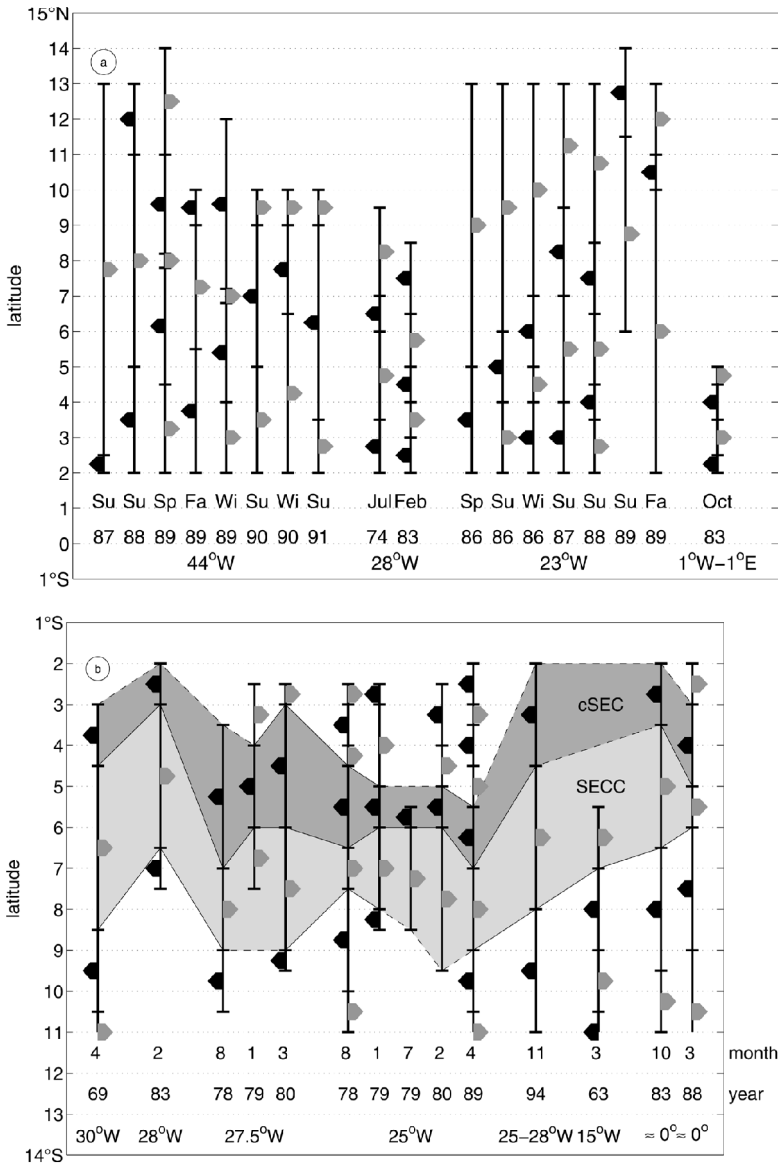


Figure 2. Composite of the direction of zonal geostrophic velocity between 800 and 900 m as derived from diverse CTD sections collected in the tropical Atlantic. (a) North of the equator. (b) South of the equator. Data sources: Chepurin and Carton (1997) for 44W and 23W. Molinari (1982) for 25W and 27.5W; level of no motion at 1000 m. Suga and Talley (1995) for 4/1989 and 2/1988. Stramma (1991) for 3/1963 and 4/1969. Institut für Meereskunde in Kiel (Polarstern Cruise ANT XII/1) for 11/1994. NODC for 7/1974 and 2/1983 at about 28W, and 10/1983 at 1W to 1E. The station spacing in these sections is 1° or less. The level of no motion for the 1974, the 1983 and the 1994 sections was set to 1500 dbar. The three lines of text at the bottom of each panel give the season or month, the year, and the longitude.

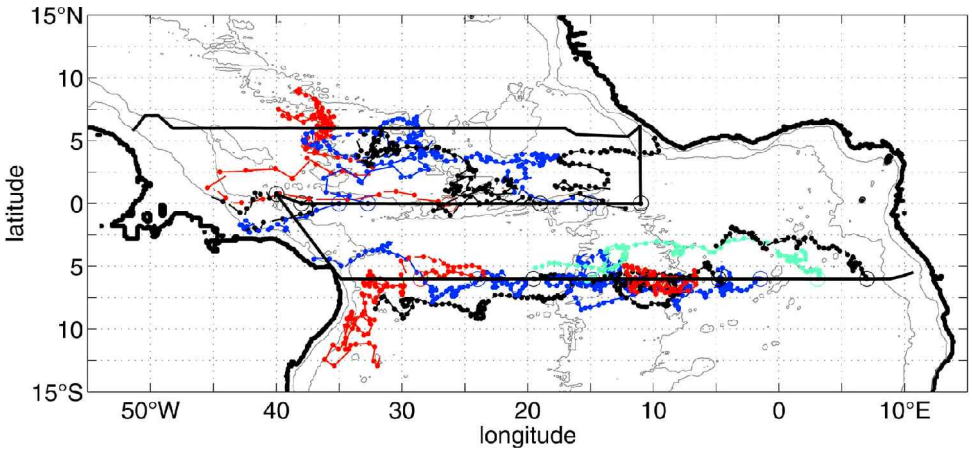


Figure 3. Trajectories of 17 PALACE floats launched in June through August 1997. The 10-day displacement vectors start at the dots. The trajectories are up to 32 months long. The colors indicate individual trajectories. The cruise track of the *RV Seward Johnson* cruise undertaken in June through August 1997 is indicated by the thick black line which crosses the tropical Atlantic three times. The isobaths are 1000 and 4000 m.

## 2. Data

As part of the Atlantic Circulation and Climate Experiment (ACCE), the last field phase of the World Ocean Circulation Experiment (WOCE), seventeen PALACE floats were launched in the summer of 1997 along the equator and 6S (Fig. 3). The first year of data was discussed by Molinari *et al.* (1999). In the present study all PALACE data obtained from July 1997 through beginning of March 2000 are analyzed. The average trajectory length is 26 months. Four of the PALACE floats ran aground on the continental shelf, three on the South American shelf and the fourth on the African shelf. These on-shelf periods, which amount to about 2% of the total number of observations, are not used in the analysis. About 64% of the useable observations are in the band 12S to 2S, and the remaining observations are between 2S and 8N.

The PALACE floats were programmed to surface after 10-day-long periods of submerged drift at a depth of nominally 1000 dbar. During their ascent to the surface a temperature profile is obtained and transmitted during a 1-day-long surface period. Afterward, the PALACE floats return to depth. The transmitted data, as well as the location information, are collected from Service ARGOS on a daily basis.

Several positions, and the corresponding times, are available for each surface period. The time lag between the first (last) surface position and the end (start) time of the submerged drift gives rise to errors of the start and end positions of the trajectory segments. The location errors depend on the surface velocity and the time lag, and can be as large as about 25 km for a current of 150 km/day and a time lag of 4 h. By extrapolation of the surface drift these errors can be reduced to about half of the distance derived without

extrapolation (see Appendix for details about the extrapolation method). The typical relationship between the 10-day submerged displacement and the 1-day displacement is about two to one. For a rather large time lag of 4 hours (at the beginning and at the end of the submerged drift) the error of the submerged velocity would be 4%. The corrected trajectories are shown in Figure 3. It should be noted that the trajectories do not represent the continuous motion of a water parcel. Due to the regular surfacing of the PALACE floats, each trajectory segment represents an individual displacement vector. The final velocity data are computed from the corrected submerged displacements.

The PALACE floats were ballasted to reach neutral buoyancy at about 1000 dbar. Initially, the equilibrium pressure was between 1017 and 1076 dbar. During the first 150 to 200 days the resting depths shoaled 100 to 200 dbar, with the equatorial PALACE floats stabilizing between 920 and 1000 dbar, and the 6S floats between 840 and 930 dbar. Throughout the study it is assumed that the trajectories are representative of the flow between 800 and 1100 dbar.

The cruise data consist of three zonal Conductivity Temperature Depth (CTD) and Lowered Acoustic Doppler Current Profiler (LADCP) sections taken along 6N, the equator and 6S (Fig. 3). Data reduction methodology for the CTD data is given in Fleurant *et al.* (1999).

Output from a global model of ocean tides was used to remove the barotropic tides from the LADCP data. The model best-fits, in a least-squares sense, the Laplace Tidal Equations and cross-over data from the first 40 TOPEX/Poseidon orbit cycles and represents an improvement to the original model described in detail in Egbert *et al.* (1994). Model/data comparisons show that the modeled harmonic constants are generally in agreement with observations, except for some disagreement primarily at the smaller constituents (Dushaw *et al.*, 1997). For the semi-diurnal tides the uncertainties are less than 10% of the amplitude. For the diurnal tides they can be a larger percentage, but the influence on the tidal current is usually weak since the amplitudes of these tides are about one order of magnitude smaller than the amplitudes of the semi-diurnal tides. Although total tidal corrections to the LADCP data can exceed  $4 \text{ cm s}^{-1}$ , the mean correction is on the order of  $1 \text{ cm s}^{-1}$ .

### 3. Intermediate depth water masses

During the PALACE float deployment along 6S the salinity minimum of the Antarctic Intermediate Water (AAIW) was found between 700 dbar and 800 dbar (Fig. 4a,  $S < 34.5$ ). The potential temperature maximum of the NADW is observed in the western basin at about 1300 dbar ( $\Theta > 4.25^\circ\text{C}$ ). The potential temperature minimum of the uCDW is found in the western basin at about 1000 dbar ( $\Theta < 4.25^\circ\text{C}$ ), between the AAIW salinity minimum and the NADW salinity maximum (Fig. 5). Although there is some controversy concerning the existence of uCDW in the tropical South Atlantic, as mentioned in the Introduction, the temperature minimum at about 1000 dbar is considered representative for this water mass.

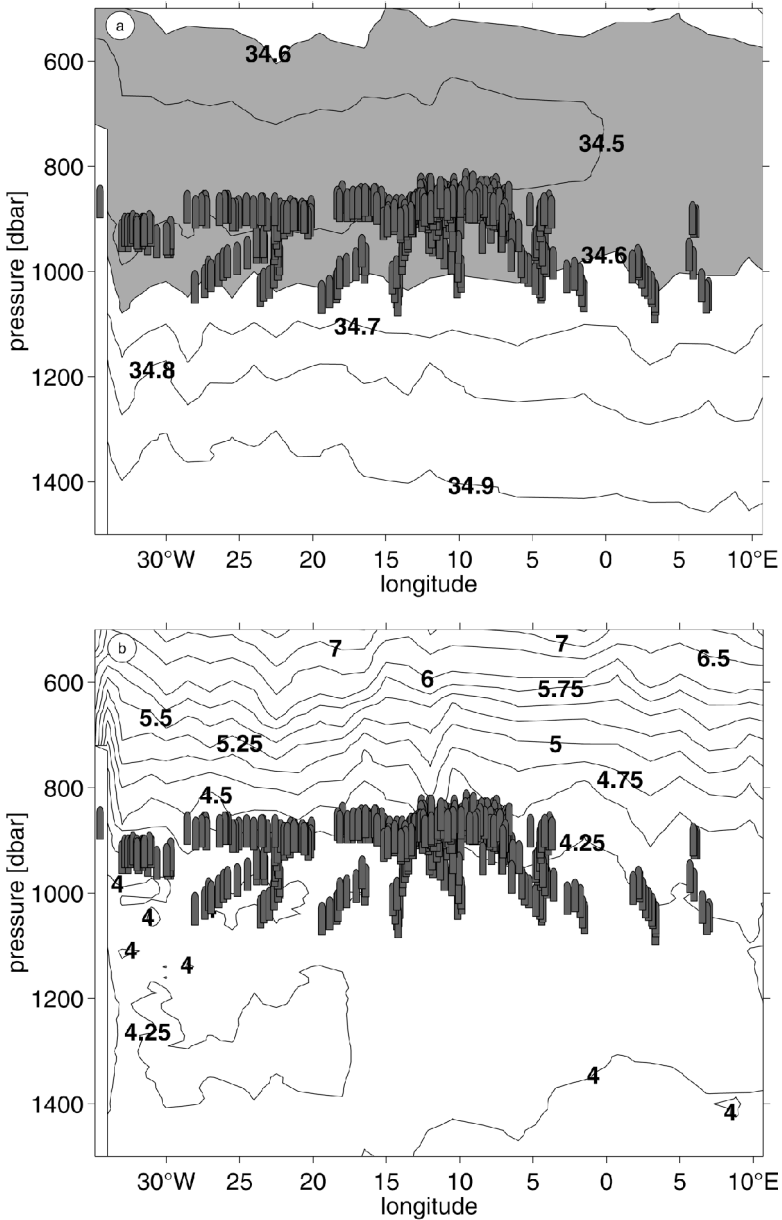


Figure 4. (a) Salinity along 6S in July 1997. The shaded area indicates the Antarctic Intermediate Water. (b) Potential temperature along the same section. The symbols are centered at the depths of the PALACE floats recorded within 1° latitude of the section.



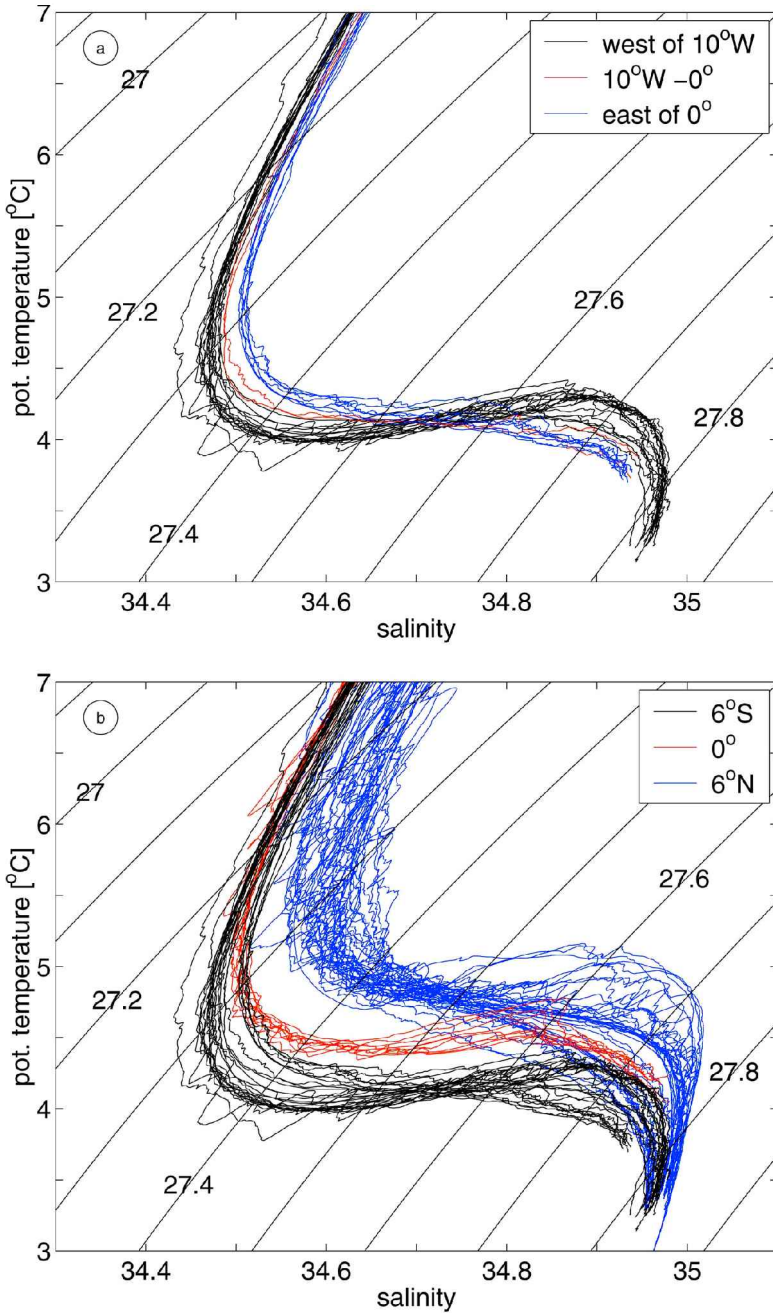


Figure 5. Potential temperature-salinity diagrams for summer 1997. (a) at 6S and (b) along all three zonal sections.

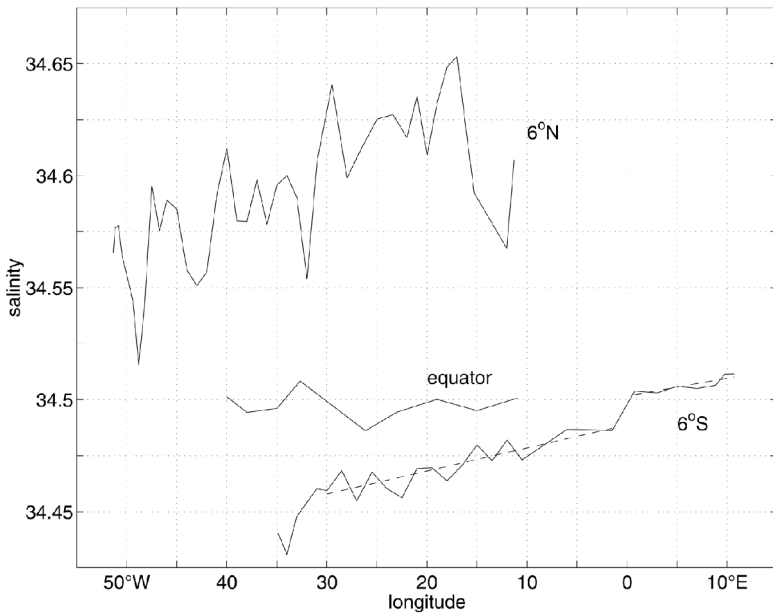


Figure 6. Salinity in the salinity minimum of the Antarctic Intermediate Water layer along three zonal sections. The two dashed lines are based on linear fits applied to two parts of the 6S section. The slopes are  $1.0 \cdot 10^{-3}/\text{degree}$  in the west and  $0.8 \cdot 10^{-3}/\text{degree}$  in the east.

The AAIW core is found along the full length of all three sections. At 6N and 6S the AAIW core salinity increases from west to east, whereas it is nearly constant at the equator (Fig. 6). At 6S a relatively sharp increase of salinity at the Greenwich Meridian is observed. This front separates the western region with higher variability superimposed on the mean slope (dashed line west of  $0^\circ$  in Fig. 6) from the eastern region with less variability. This front coincides with the simultaneous observation of an oxygen front (not shown). At 6N the variability of the salinity is much stronger than at 6S but there is no sign of a front.

A striking similarity of the minimum salinity at the equator and at the eastern end of the 6S section is observed in Figures 5 and 6. The potential temperature salinity diagram reveals overlapping curves in the AAIW (in the potential temperature range  $4.5^\circ\text{C}$  to  $5^\circ\text{C}$ ) for the eastern ends of the 6S and the equatorial sections. In the west the AAIW salinity increases by about 0.05 between 6S and the equator. Between the equator and 6N the northward salinity increase outside of the western boundary regime is about twice as large as between 6S and the equator.

Initially the PALACE floats drifted at about 1000 dbar, within the uCDW at 6S and just below the AAIW at the equator. Due to shoaling, the 6S PALACE floats were located in the lower half of the AAIW after the first few months of the trajectories. The equatorial PALACE floats experienced less shoaling and thus stayed below the AAIW throughout their mission.

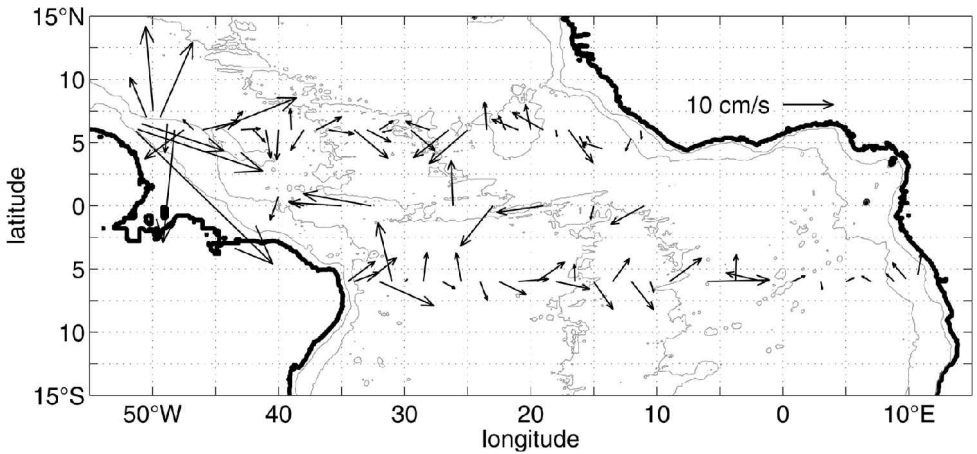


Figure 7. Vectors of mean velocity between 800 and 1100 m as measured with a LADCP during the summer 1997 cruise. The velocities have been corrected for the barotropic tides. The isobaths are 1000 and 4000 m.

#### 4. The circulation pattern

##### a. Initial conditions

The intermediate depth velocity vectors for summer 1997 (Fig. 7) are derived from the LADCP velocities by averaging the velocity between 800 m and 1100 m. Along 6S the zonal flow is predominantly eastward west of 5W ( $3.9 \pm 3.7 \text{ cm s}^{-1}$ ), whereas no clear preference of east- or westward flow can be discerned east of 5W ( $-0.9 \pm 3.0 \text{ cm s}^{-1}$ ). The values in the parenthesis are the mean and the standard deviation derived from the vectors in Figure 7. The zonal equatorial flow is predominantly westward ( $-5.7 \pm 4.6 \text{ cm s}^{-1}$ ). At 6N the mean zonal velocity is eastward west of 29W ( $4.4 \pm 8.3 \text{ cm s}^{-1}$ ) and westward east of this longitude ( $-1.8 \pm 3.7 \text{ cm s}^{-1}$ ), but the preference of the flow directions is weaker than at 6S and at the equator. It is also noted that zonal velocities exceeding  $10 \text{ cm s}^{-1}$  are only observed west of 44W at 6N (in the western half of the western basin), whereas such a distribution is not apparent at 6S.

The off-equatorial sections cover the eastern and western boundary regions. These sections reveal equatorward flow at both boundaries. At 6N a strong northward current is observed just east of the intense southward flow along the western boundary. Significant meridional flow is also recorded in the interior at many locations along all three sections. In these cases the meridional velocity can be more than twice as large as the zonal velocity. For example, at the equator four locations with meridional velocities greater than or equal to the zonal velocities are observed (15W, 23W, 26W, 40W, Fig. 7).

At 6S a comparison of the LADCP velocity with the first 10-day displacement of the PALACE floats shows a good agreement of flow directions. The correlation coefficients between LADCP and initial PALACE float velocities are 0.62 and 0.70 for the zonal and

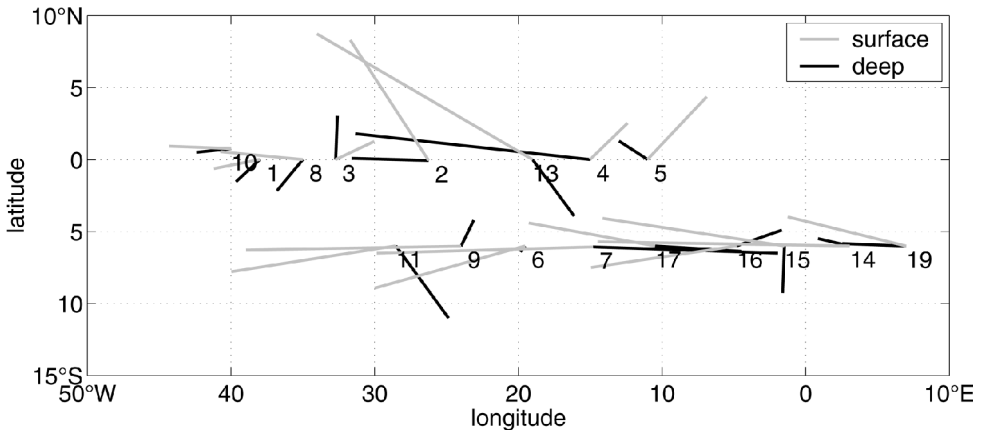


Figure 8. Surface (gray) and submerged (black) total displacements of the PALACE floats. They are based on the full record length of each PALACE float. The displacement vectors start at the first position of the trajectories (indicated by the numbers).

meridional components, respectively. At the equator, the independent velocity observations are not correlated (the correlation coefficients are 0.49 for zonal motions and  $-0.30$  for meridional motions). This could be an indication of larger variability and/or smaller time scales at the equator.

#### b. The PALACE float trajectories

Three visual impressions about the large-scale mean flow result from viewing all the trajectories shown in Figure 3. First, there are large zonal displacements in the trajectories; second, none of the instruments launched at 6S reached the equator during the more than 2.5-year-long period; and third, there is a net northward drift north of the equator. These first impressions might be misleading since the overall displacement of a PALACE float is a combination of the drifts at the resting depth and at the surface. The contributions of these two components are shown in Figure 8. About half of the instruments reveal opposing directions of one or both velocity components between the surface and intermediate depth (800 to 1100 dbar).

Seven of the eight PALACE floats deployed on the equator exhibit net northward surface flow (Fig. 8). The occurrence of southward or northward submerged displacements is evenly distributed (four northward, four southward), which is mainly due to the shortness of trajectories 1, 8 and 10. These PALACE floats were on the shelf after about 100 days and stayed there for at least three quarters of their remaining life. A clear preference for northward submerged flow emerges if the displacements of these three PALACE floats are disregarded (four northward, one southward). PALACE 1 and 10 would eventually have enhanced the domination of the northward drift because they were caught in the Intermediate Western Boundary Current (IWBC) before they ran aground

after only two cycles in that current (not shown). Of the five instruments that worked for at least 470 days without running aground, only PALACE 13 experienced opposing meridional displacements at the surface and at depth. For this PALACE float and also for PALACE 2 the meridional displacement is dominated by the periods at the surface. PALACE 8 and 3 indicate a bifurcation of the EIC. Their trajectories are not shown in detail, but they can be found in blue in Figure 3, starting at 35W and 32.7W, respectively. PALACE 8 experienced a 1-month-long southwestward submerged drift. During the same period PALACE 3 drifted northwestward.

At 6S the occurrence of southward or northward displacements at the surface and at depth are nearly evenly distributed (four northward, five southward, Fig. 8). Eastward and westward submerged displacements also occur with similar frequencies, whereas the mean zonal surface displacement is always westward. The meridional surface displacement shows a regional dependence. It is predominantly northward in the eastern basin (east of 12W) and mostly southward in the western basin, whereas the meridional submerged displacement does not depend on the longitude of deployment. It is also noted that opposing displacements at the two drift levels are recorded by four of the nine instruments (all of them lived for at least 600 days). This differs from the equatorial observations where significant opposing displacements occurred only once. It is also noted that the northward surface displacements at the equator can be more than twice as large as at 6S. Both factors, and also the slight preference for southward submerged displacements, explain why the 6S PALACE floats do not reach the equator.

### *c. The mean flow and its variance*

The PALACE float data were used to estimate the mean and the standard deviation of the submerged velocity in  $2^\circ$  latitude by  $5^\circ$  longitude boxes (Fig. 9). Only results based on at least three velocity estimates are shown (i.e., a minimum of 30 days of observation). The question arises if three observations are sufficient for a statistically sound result. The Lagrangian time scales are necessary to answer this question. Nine RAFOS trajectories obtained by Institut für Meereskunde Kiel and published by Boebel *et al.* (1999b) are used as part of this study to estimate the time scales. The instruments drifted in the AAIW layer in the tropical Atlantic, and their position was recorded daily. The derived zonal time scales range from 5 to 27 days. Some auto-correlation functions have one extreme value, and others have many extreme values. Those with one extreme value have a time scale of less than 12 days, and the mean is  $7.5 \pm 2.5$  days. The others have a time scale exceeding 12 days, and the mean is  $18.8 \pm 6.1$  days. The mean over all time scales is  $12.5 \pm 7.2$  days, which is only slightly longer than the duration of 11 days of the PALACE float cycle. This result, together with the fact that the PALACE floats go through a 1-day surface period in each cycle, indicates that each velocity derived from a submerged displacement can be seen as statistically independent, even though the range of possible time scales is quite large. It is important to note here that the statistical independence of the velocity measurements does not mean that the box averages represent annual means. The observa-

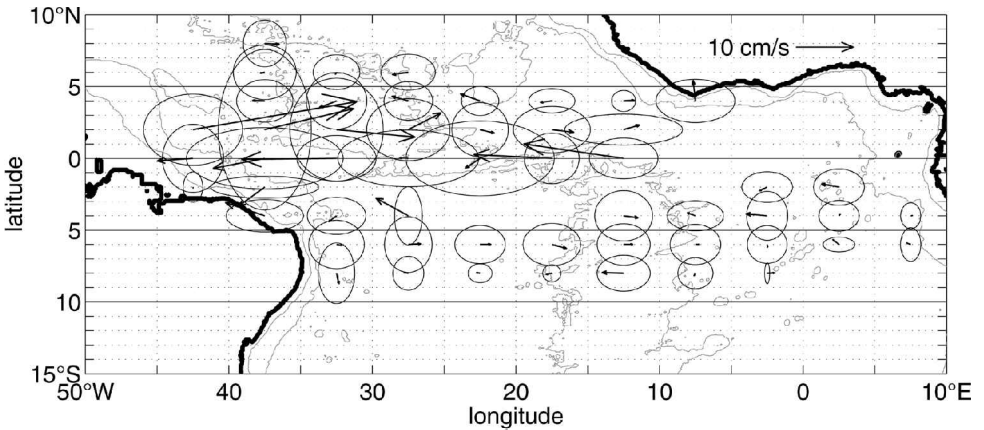


Figure 9. Mean velocities and standard deviations in  $2^\circ$  (latitude) by  $5^\circ$  (longitude) boxes derived from the PALACE trajectories presented in Figure 3. Only boxes with at least three velocity estimates are shown. The isobaths are 1000 and 4000 m.

tions of the flow along the equator are based on little more than half a year of data, most of which were obtained during the season of westward flow. Similarly most observations in 1N to 3N are from a half-year period (September–March), as only one PALACE float stayed in the latitude band until January 1999. Between 3N and 6N, and between 4S and 8S, the temporal coverage is much better (nearly two years of data are available).

Three flow regimes can be discerned in Figure 9: a region of high velocities (box averages up to  $28 \text{ cm s}^{-1}$ ) on and just north of the equator and two regions of lower velocities (box averages mostly less than  $5 \text{ cm s}^{-1}$ ) north and south of this equatorial band. On average the absolute zonal velocity for the boxes at the equator and at 2N is about  $10 \text{ cm s}^{-1}$ . For the boxes at and north of 4N the result is about  $2 \text{ cm s}^{-1}$ . Occasionally zonal velocities exceeding  $10 \text{ cm s}^{-1}$  are observed north of 4N in the PALACE float data, but only west of 25W (not shown). In the equatorial band the zonal velocity frequently exceeds  $10 \text{ cm s}^{-1}$  and sometimes is larger than  $30 \text{ cm s}^{-1}$ . The transition from the high-velocity equatorial regime to the low-velocity regime farther north depends on the longitude. It is located near 3N west and near 2N east of 25W. The southern extent of the high velocity equatorial regime cannot be defined due to the sparse data coverage between the equator and 5S. The off-equatorial bands exhibit zonal standard deviations that are generally twice as high as the means, whereas the zonal standard deviations near the equator are typically smaller than the means. The lower variability in the equatorial band may be partly due to the short record length of about 5 months in both the westward and the eastward current. The mean meridional velocities are nearly always smaller than the zonal velocities. This is obviously quite different from the results of the one-time survey (Fig. 7). The zonal velocities derived from the independent data sets are similar (Figs. 7 and 9).

Mean westward velocities in the EIC as recorded by individual PALACE floats vary

Table 1. Zonal velocities in the Equatorial Intermediate Current (EIC) and the Northern Intermediate Countercurrent (NICC) from the PALACE floats.  $\hat{u}$  is the maximum zonal velocity and  $\bar{u}$  is the mean  $\pm$  standard deviation of the zonal velocity. The time period of observation is given in the last column.

EIC					
PALACE	Longitude	Latitude	$\hat{u}$ [cm s <sup>-1</sup> ]	$\bar{u}$ [cm s <sup>-1</sup> ]	Date
10	45–43W	$\pm 1^\circ$	-11.6	$-11.2 \pm 0.6$	28.09.1997–19.10.1997
2	44–26W	$\pm 1^\circ$	-32.4	$-16.8 \pm 7.9$	22.07.1997–19.11.1997
8	38–35W	$\pm 1^\circ$	-20.7	$-15.9 \pm 6.8$	23.07.1997–13.08.1997
3	36–33W	$\pm 1^\circ$	-18.9	$-12.0 \pm 6.0$	23.07.1997–24.08.1997
13	27–19W	$\pm 1^\circ$	-14.0	$-8.6 \pm 3.1$	20.07.1997–17.11.1997
4	21–15W	$\pm 1^\circ$	-20.6	$-14.9 \pm 4.3$	19.07.1997–31.08.1997
5	17–11W	$\pm 1^\circ$	-21.9	$-15.7 \pm 5.8$	18.07.1997–30.08.1997
NICC					
PALACE	Longitude	Latitude	$\hat{u}$ [cm s <sup>-1</sup> ]	$\bar{u}$ [cm s <sup>-1</sup> ]	Date
2	45–32W	1–4N	34.0	$19.3 \pm 8.0$	20.11.1997–20.03.1998
3	36–28W	1–3N	26.2	$14.6 \pm 7.3$	05.09.1997–12.12.1997
13	27–21W	0–2N	21.2	$14.7 \pm 5.9$	10.12.1997–07.03.1998
4	22–19W	1–2N	9.2	$7.6 \pm 1.4$	26.10.1997–08.12.1997
5	18–13W	1–2N	15.2	$9.3 \pm 3.0$	03.10.1997–29.12.1997

between  $8.6 \text{ cm s}^{-1}$  and  $16.8 \text{ cm s}^{-1}$ , with a maximum of more than  $30 \text{ cm s}^{-1}$  (Table 1). The average of all mean westward EIC velocities of the seven PALACE floats is  $-13.6 \pm 3.0 \text{ cm s}^{-1}$ . The range of the zonal velocity in the NICC (in 1N to 3N) is similar to that found in the EIC. Means vary between  $7.6 \text{ cm s}^{-1}$  and  $19.3 \text{ cm s}^{-1}$  and the highest velocity again exceeds  $30 \text{ cm s}^{-1}$ . The average of all mean NICC velocities of the five PALACE floats is  $13.1 \pm 4.7 \text{ cm s}^{-1}$ . This average cannot be seen as a valid estimate for the NICC velocity across the Atlantic since the data indicate a longitudinal dependence of the zonal velocity (Fig. 10a). West of the 28W the velocity in the NICC is nearly twice as large ( $16.2 \pm 2.7 \text{ cm s}^{-1}$ , three PALACE floats) as farther east ( $8.5 \pm 1.2 \text{ cm s}^{-1}$ , two PALACE floats). In the western basin the zonal velocity frequently exceeds  $20 \text{ cm s}^{-1}$ , whereas these high velocities are not observed in the eastern region (Fig. 10b). The trajectory of PALACE 2 (Fig. 11a, blue) indicates that a longitude dependence of the zonal velocity might exist inside the western basin. It drifted with a velocity of up to  $35 \text{ cm s}^{-1}$  from 45W to 32W, with the largest 10-day displacements occurring west of 40W.

Around 6S the mean flow derived from the PALACE float data (Fig. 9) is eastward (SECC) west of 5W as during the deployment cruise (Fig. 7). At 8S and 4S most boxes have westward mean velocities (Fig. 9). The overall means are  $-0.6 \pm 1.6 \text{ cm s}^{-1}$  at 8S,  $0.9 \pm 1.3 \text{ cm s}^{-1}$  at 6S, and  $-2.0 \pm 3.1 \text{ cm s}^{-1}$  at 4S. East of 5W the mean velocities are westward or weakly eastward between 7S and 1S (Fig. 9), with a mean of  $-1.2 \pm 1.5 \text{ cm s}^{-1}$ . It is also noted that the sign of the zonal velocity changes near this longitude between 9S and 3S. This flow pattern agrees well with the observations obtained in summer 1997 (Fig. 7).

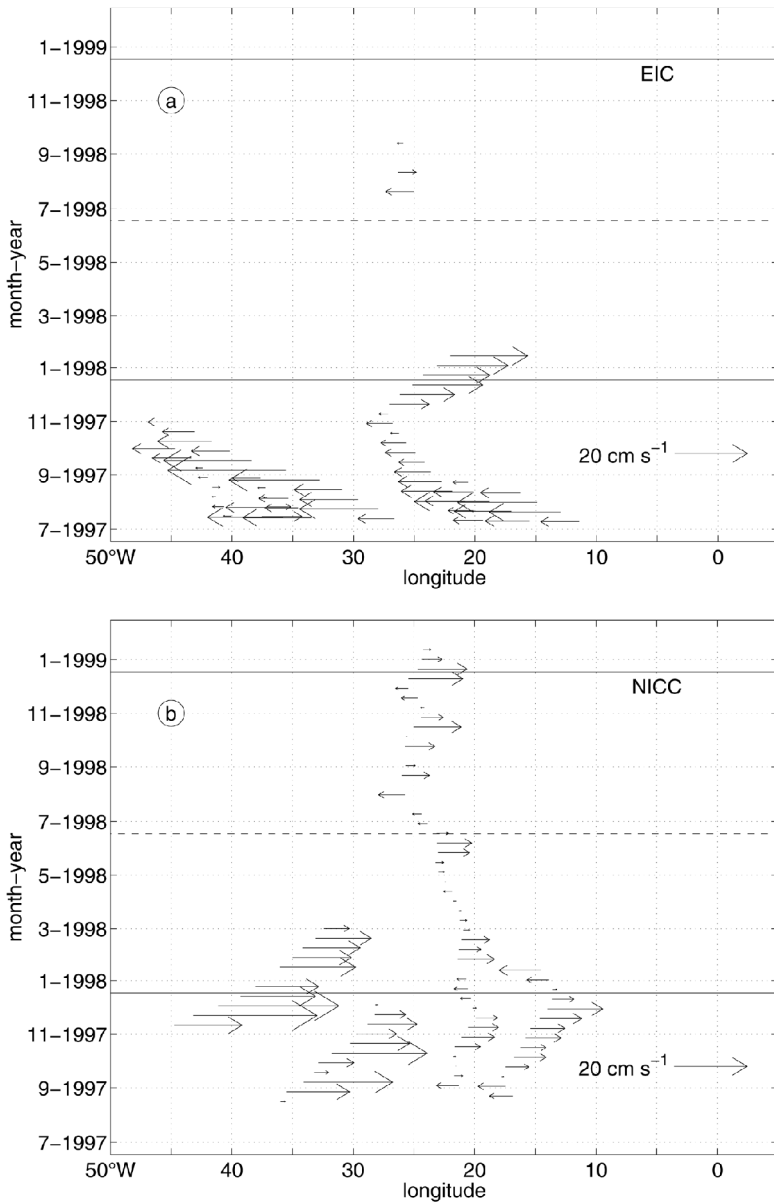


Figure 10. Zonal velocity vectors from the PALACE data (a) in the EIC (1S to 1N) and (b) in the NICC (1N to 3N).

Velocity distributions in latitude bands are shown in Figure 12 to illustrate further the mean flows and the variability. The panel shows that the probability for eastward velocities (SECC) at intermediate depth is largest around 6S (68%), and somewhat lower at 7.5S to



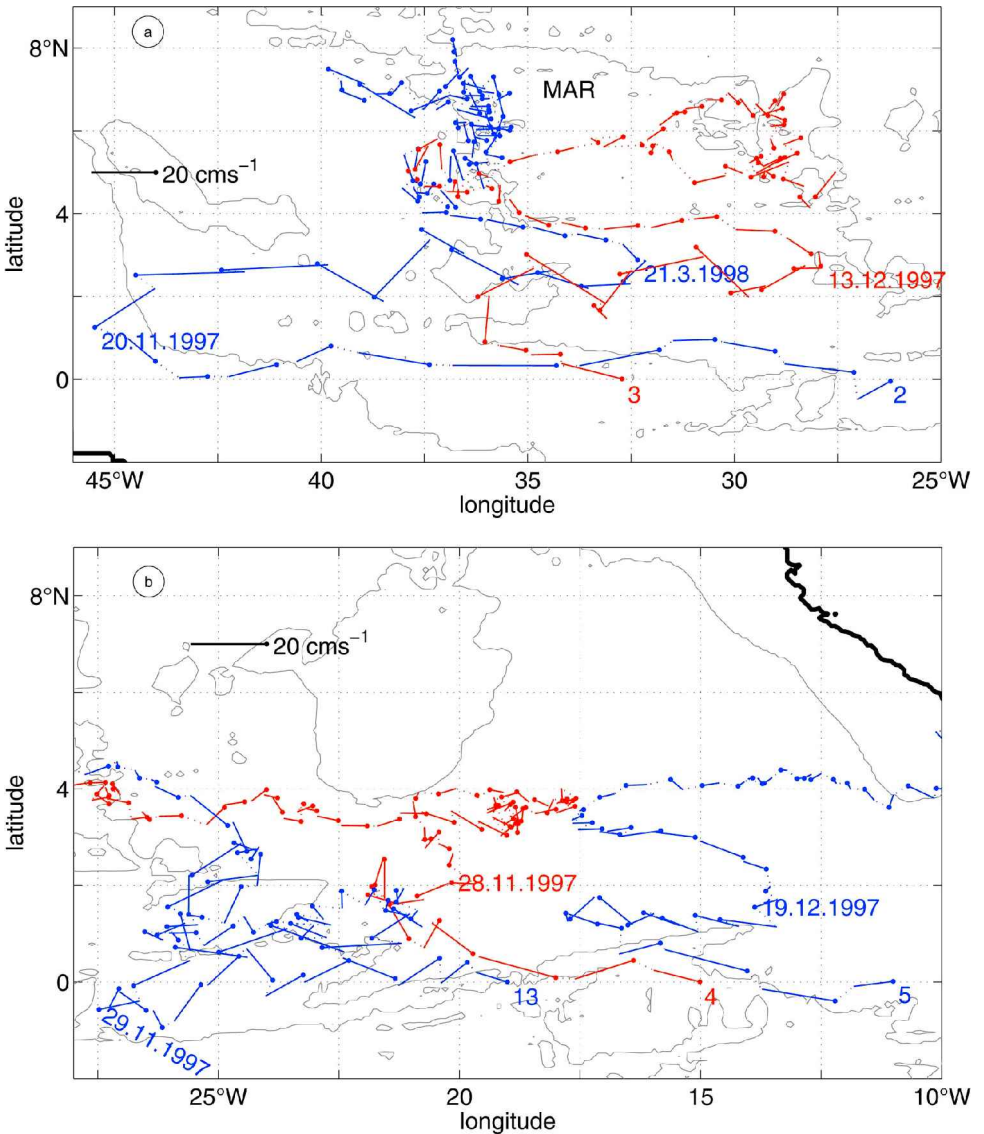


Figure 11. Example trajectories for the PALACE floats. The 10-day displacement vectors start at the dots. (a) and (b) show trajectories at and north of the equator.

6.5S (56%). Farther north, westward velocities dominate the picture. The maximum probability for westward flow (cSEC) is found between 4S and 2S (62%), followed by 5.5S to 4S (55%). The transition latitude between the two currents can be anywhere between 6.5S and 4S. It is important to note that the flow north of 5.5S is relatively poorly sampled. Most of the observations were obtained east of 15W or west of 25W. Nevertheless, it can

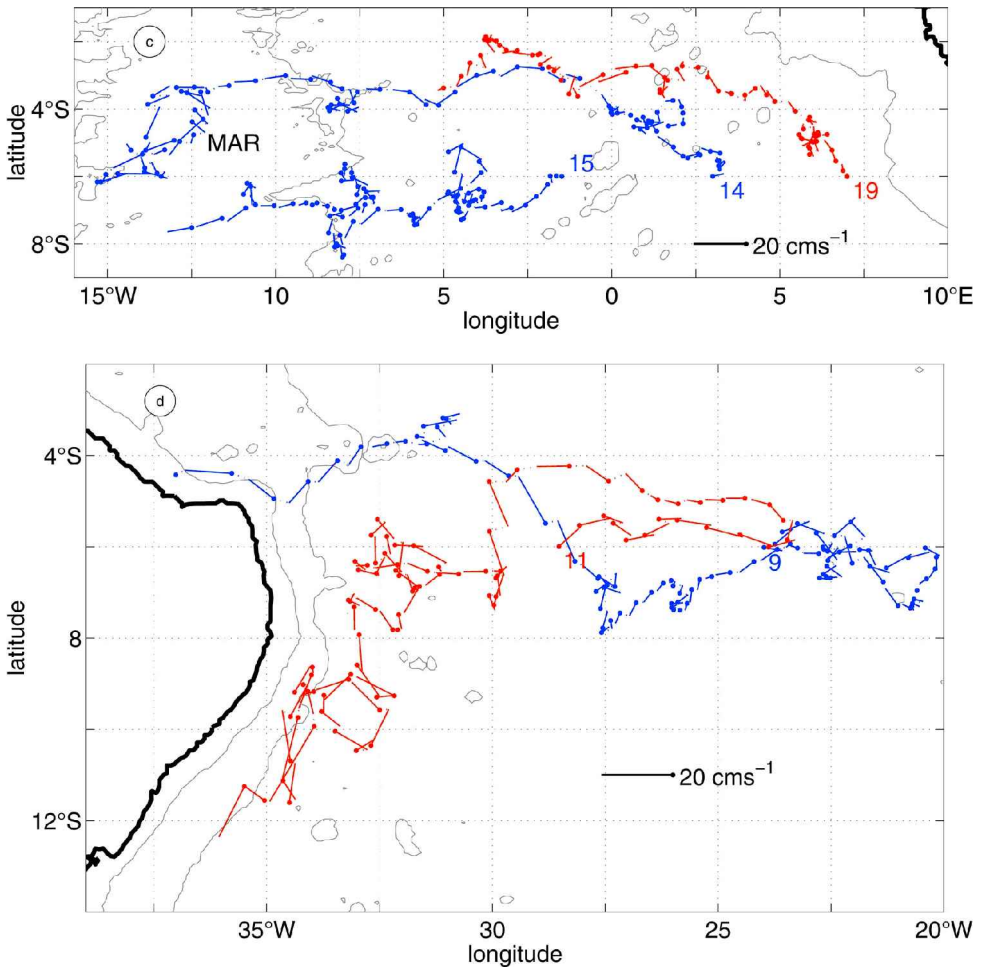


Figure 11. (c) and (d) show trajectories south of the equator. The 4000 m isobath is shown. (d) also shows the 1000 m isobath. MAR indicates the Mid-Atlantic Ridge.

be assumed that the distributions deliver a realistic representation of the basin-wide flow pattern. This assumption is based on the fact that the mean zonal flow between 25°W and 15°W at 6°S and at 8°S is of the same direction as in the adjacent boxes east and west of this region.

#### d. Temporal and regional variability of zonal currents

Figure 10 shows the zonal component of the submerged PALACE float velocities between 1°S and 1°N and between 1°N and 3°N. The PALACE floats launched along the equatorial section experienced persistent westward drift between 1°S and 1°N for several months after their deployment (Fig. 10a), consistent with the westward flow observed

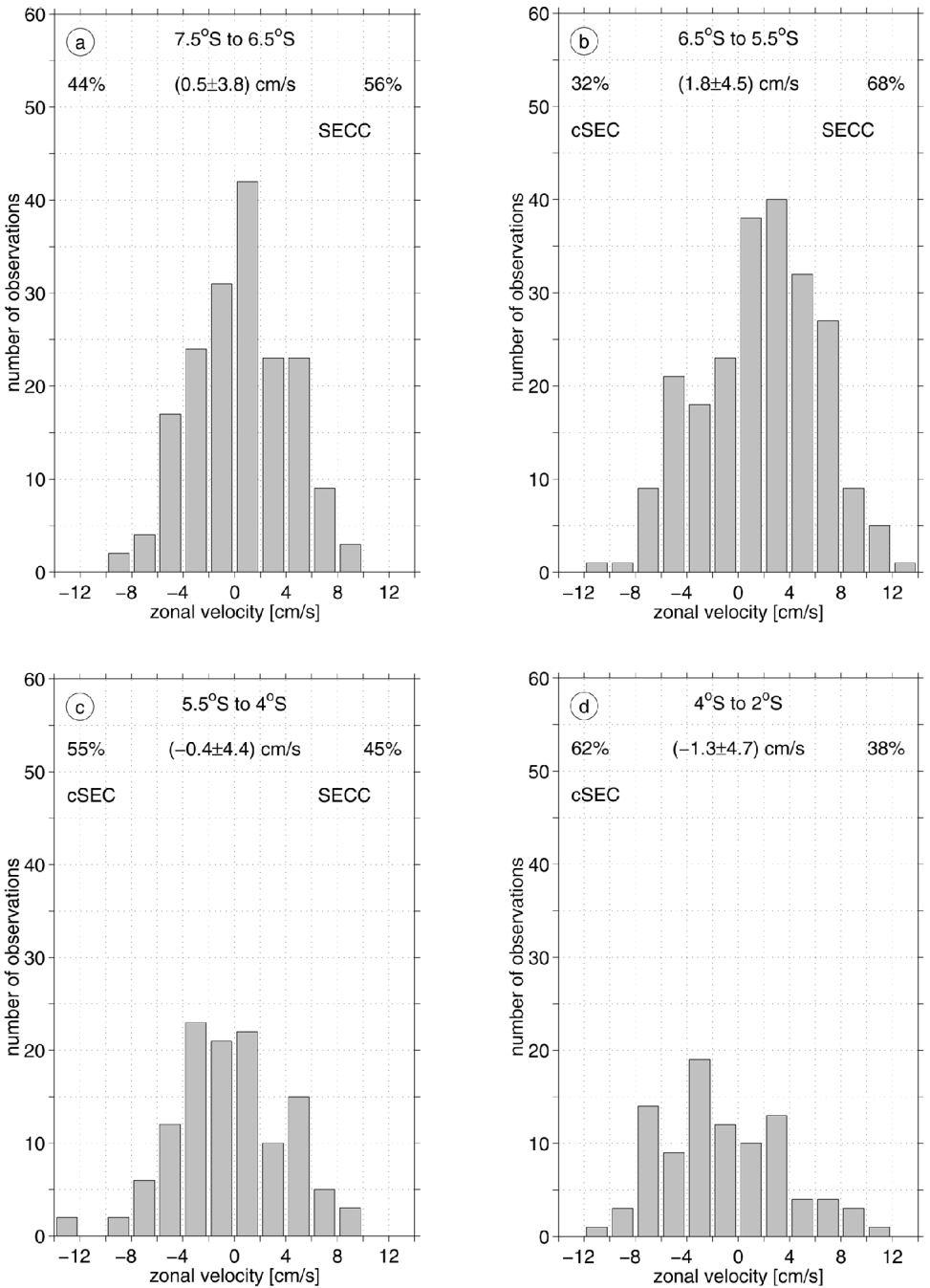


Figure 12. Distribution of zonal velocity derived from the PALACE trajectories. The numbers in the left (right) corners give the percentage of negative (positive) velocities. The numbers in the middle are the means and the standard deviations of the velocities.

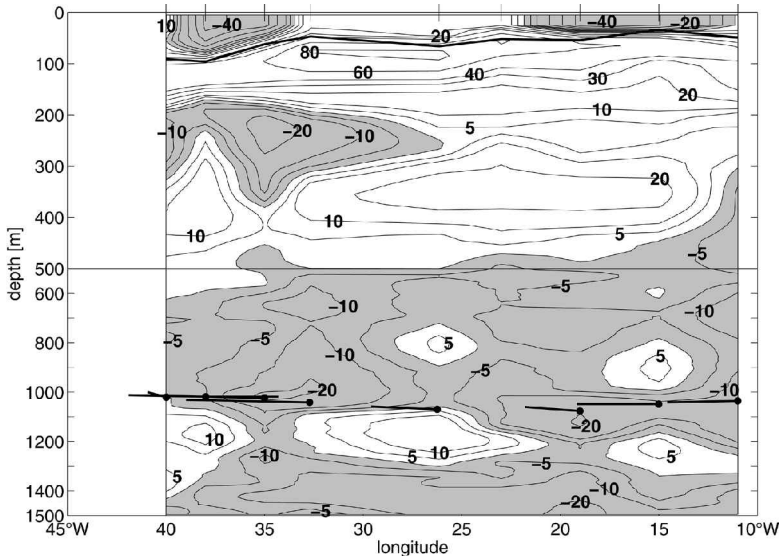


Figure 13. Zonal velocity from the LADCP data at the equator in summer 1997. The velocity has been corrected for the barotropic tides. Tick marks at the top indicate the stations. The initial velocities of the PALACE float are shown as black lines starting from the black dot ( $5^\circ$  correspond to  $15 \text{ cm s}^{-1}$ ).

during the deployment week, 18 to 25 July 1997 (Fig. 13). Only PALACE 13 shows a drift reversal in this latitude range at the end of November 1997. It reveals eastward drift near  $1^\circ\text{N}$  (Fig. 11b) until the end of January 1998 (Fig. 10a).

Figure 10b indicates a change in the NICC strength. The largest velocities occur from September 1997 to January 1998 in the western basin. In March 1998 the velocity becomes very small between  $20^\circ\text{W}$  and  $25^\circ\text{W}$ . Between this time and January 1999 the sign and magnitude of the zonal velocity changes frequently. These observations are based on PALACE 13, which is the only PALACE float that stayed in the latitude band of the NICC. It is noted that even before March 1998 the zonal flow in the same longitude band,  $20^\circ\text{W}$  to  $25^\circ\text{W}$ , was alternating. These observations are from PALACE 4.

Individual trajectories (Figs. 11a and b) indicate some correlation of current reversals at and north of the equator. At the end of November 1997 two PALACE floats experienced nearly simultaneous reversals of the zonal drift (Fig. 11b): Trajectory 13 indicates a reversal of the equatorial flow near  $28^\circ\text{W}$  (see above), and the eastward drift of PALACE 4 terminates near  $20^\circ\text{W}$ . Two more PALACE floats experience reversals from eastward to westward drift around mid December 1997: PALACE 3 at  $28^\circ\text{W}$  (Fig. 11a) and PALACE 5 at  $13^\circ\text{W}$  (Fig. 11b). Trajectory 2 reverses much later, in March 1998 (Fig. 11a). Most of the reversals coincide with meridional displacements of the PALACE floats by  $1^\circ$  or more, which can be due to the surface drift and/or the submerged drift. This northward displacement is probably the main cause for the reversals. For example, PALACE 4 and 5

(Fig. 11b) show weakening and finally reversed flow as they are displaced to the north. It is also noted that the westward drift after the reversals is observed between 3N and 4N.

As described in Section 4c the mean flow in the tropical South Atlantic, south of about 2S, is generally weak and mostly westward east of the Mid-Atlantic Ridge. Three trajectories in this area are shown in Figure 11c. Superimposed on the overall westward submerged drift are shorter periods of eastward and meridional motions. These perturbations frequently take the form of eddy-like motions (e.g. 5S, 6E/4S, 2E/6S, 4W/4S, 13W). These events can last up to 8 months. Their duration might be influenced by the combined effects of surface and submerged drift. The surface flow of individual PALACE floats launched in the eastern basin at 6S is mostly westward throughout their mission (between 73% and 91% of the zonal surface velocities are westward), whereas the zonal submerged drift alternates (between 41% and 56% of the zonal submerged velocities are westward). A similar 5-month-long event is visible in a RAFOS trajectory at 15W 6S (Boebel *et al.*, 1999b, their Fig. 1b). This indicates that the pattern is not simply a result of the regular surfacing of the PALACE floats. However, the combined effect of eastward submerged and westward surface flow might increase the residence time of a PALACE float in such a perturbation. The meridional extents of the perturbations are between 100 and 300 km, and their zonal extents are between 100 and 200 km. The larger meridional undulations occur primarily during events with 7 to 8 month duration (e.g. near 5W and 8W in Fig. 11c). The time series of the zonal velocity in Figure 14, which is based on three PALACE floats, shows that eastward flow seems to preferably occur in summer/fall in the region bounded by 6.5S to 5.5S, 15W to 5W.

#### *e. Meridional flow near the boundaries*

The trajectories of PALACE 14 and 19 (Fig. 11c) reveal northward flow parallel to the eastern boundary from 6S to about 3S. Their mean meridional velocities for the initial periods of steady northward drift are  $1.4 \pm 0.8 \text{ cm s}^{-1}$  (7 cycles) and  $3.0 \pm 1.5 \text{ cm s}^{-1}$  (4 cycles), respectively. The mean meridional velocities for the whole period of net northward drift are  $0.7 \pm 1.8 \text{ cm s}^{-1}$  (33 cycles) and  $0.4 \pm 2.6 \text{ cm s}^{-1}$  (25 cycles).

Trajectories 9 and 11 (Fig. 11d) captured the westward flow in the cSEC between 5S and 4S. PALACE 11 turns south at 4S 30W and makes its way to 12S, with considerable mesoscale motions (the mean meridional velocity after it started the southward motion in May 1999 is  $-2.1 \pm 8.6 \text{ cm s}^{-1}$ ). At a later time PALACE 9 crosses the path of PALACE 11 near 30W and continues westward until the PALACE float is captured by the NBUC. After two cycles in this current the instrument is trapped on the shelf. The mean speed during these two cycles is  $11.2 \pm 3.0 \text{ cm s}^{-1}$ . Some PALACE floats reached the western boundary near the equator and turned north in the IWBC (not shown in detail). Similar to the fate of PALACE 9, it did not take long before they were also trapped on the shelf.

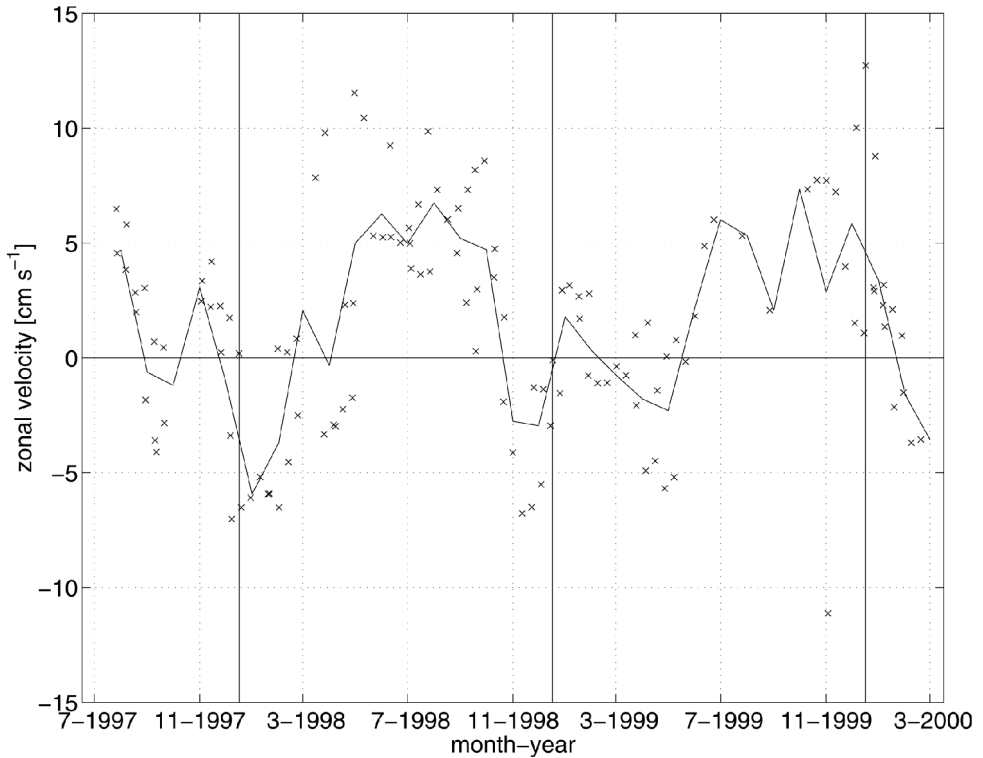


Figure 14. Time series of zonal velocity (crosses) in the region 6.5S to 5.5S, 15W to 5W based on all PALACE floats in the region (number 15, 16 and 17). The solid line gives the monthly means. The vertical lines mark the end of each year.

#### f. Meridional flow in the interior

The trajectories of the equatorial PALACE floats reveal significant meridional displacements in the interior (Figs. 11a and b). Those of PALACE 2 and 3 (Fig. 11a) are particularly large ( $2^\circ$  or more) as they switch from the EIC to the NICC in the western basin. Trajectory 13 (Fig. 11b) differs from the other equatorial trajectories (2 to 5) revealing frequent changes in the meridional velocity on its way to the west (Fig. 15). The period of this meander-like variability is 30 to 45 days. PALACE 2 and 3 (Fig. 11a) experience similar changes of meridional drift in the NICC with a similar period (PALACE 3 is shown in Fig. 15). Both of them leave the NICC to the north and drift west near 4N, before turning north once again, between 35W and 38W (Fig. 11a). In the eastern basin (Fig. 11b) meridional displacements from the EIC to the NICC are mostly smaller than in the western basin (less than  $1^\circ$ ), and the transition from the NICC to the westward current between 3N and 4N is not as smooth as in the western basin, where trajectories 4 and 13 reveal a period of variable flow before starting to move westward. Trajectory 5 moves

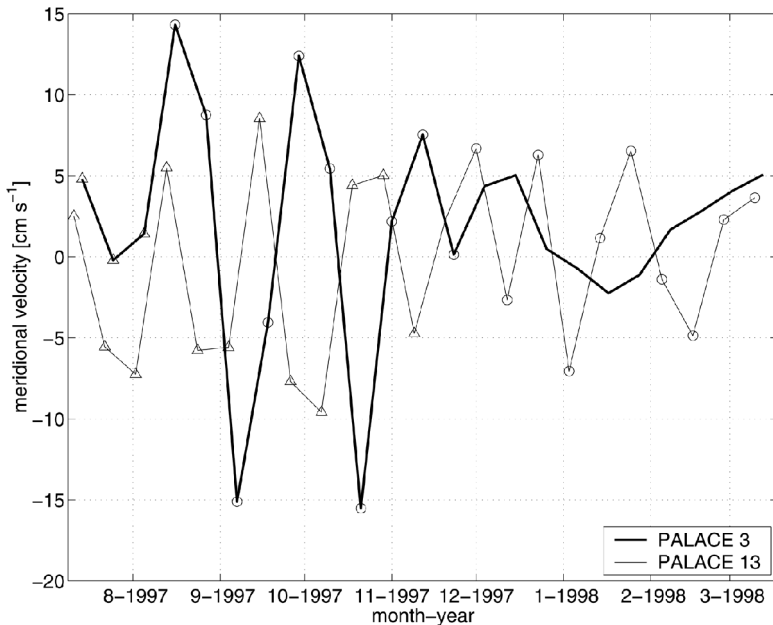


Figure 15. Meridional velocity in the EIC and the NICC for PALACE 3 and PALACE 13. Triangles indicate all estimates in the EIC, circles mark all estimates in the NICC.

quickly from one current to the next at 13W (similar to the situation in the western basin), but the transition is strongly influenced by the surface flow.

## 5. Discussion

Between 8S and 6N six zonal bands of mean eastward or westward velocity can be identified in the recent Lagrangian observations (black bars in Fig. 16). In contrast to this, Stramma and Schott (1999) showed eight currents (gray bars in Fig. 16). The eastward current at 2S is missing in the present observations due to a lack of data.

At and north of the equator, the Lagrangian observations are in good agreement with the Stramma and Schott (1999) result (Fig. 16). It is noted, however, that the westward flow at 6N derived from the present Lagrangian observations is based on a relatively small amount of data and that eastward zonal flow dominates along the western part of the 6N section taken in summer 1997 (Fig. 7). Significant westward zonal flow is only found along the eastern part of the section (east of 28W), and in the 30W to 25W box at 6N (Fig. 9). Figure 2a shows that the direction of the zonal flow at 6°N depends on the time and longitude of observation. At 23W, 6N (in the eastern basin) eastward flow was observed more often than westward flow. At 44W, 6N (in the western basin) east- and westward flow were observed equally often. The distribution in the western basin is supported by the very small mean velocities in the 6N boxes west of 30W (Fig. 9). Molinari *et al.* (1999) presented

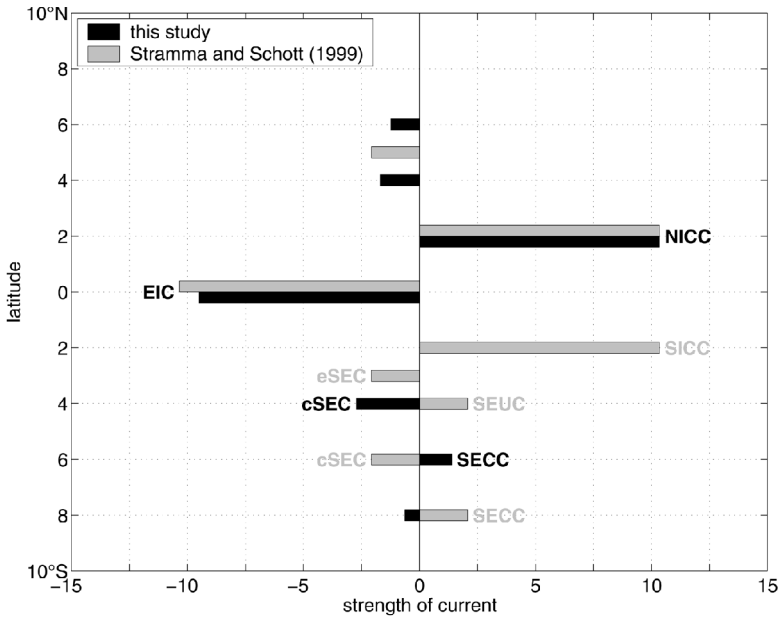


Figure 16. Schematic of the zonal flow at intermediate depth from Stramma and Schott (1999) and from the present study. For the Stramma and Schott (1999) results (Fig. 1) the strength of the current is only an approximation which differentiates between strong and weak currents. For the results from this study the current strength is the mean zonal velocity in cm/s derived from the box averages shown in Figure 9. The three black bars at and south of 4S do not include data east of the Greenwich Meridian. The bars at the equator and at 2N were shifted meridionally to prevent overlapping. The abbreviations are: Northern Intermediate Countercurrent (NICC), Equatorial Intermediate Current (EIC), Southern Intermediate Countercurrent (SICC), South Equatorial Current (SEC), equatorial SEC (eSEC), central SEC (cSEC), southern SEC (sSEC), South Equatorial Undercurrent (SEUC), and South Equatorial Countercurrent (SECC).

PALACE float trajectories in the area bounded by 5N and 7N, 38W and 48W which indicate that the small means with high standard deviations might be due to a seasonal change of the flow. Their trajectories show a preference for eastward flow from August 1997 through February 1998. In February through April 1998 the flow is westward, followed by a 4-month period of weak eastward drift. All these observations indicate that the basin-wide westward flow proposed by Stramma and Schott (1999) might not be of a permanent nature.

South of the equator the recent observations do not support the number and meridional locations of the zonal currents proposed by Stramma and Schott (1999, Fig. 16). The Lagrangian data reveal mean westward flow at 8S, mean eastward flow at 6S (SECC), and mean westward flow at 4S (cSEC, Figs. 9 and 16). Stramma and Schott (1999) suggested that two additional currents exist between the cSEC and the SICC: The South Equatorial Undercurrent (SEUC) and the equatorial SEC (eSEC). The observations at 25W in Figure



2b show several alternating flow bands north of the cSEC, which supports the eSEC/SEUC hypothesis. But the PALACE trajectories presented here do not support such a flow pattern. The currents south of the SICC do not extend across the whole basin. The SECC and the current at 8S are only present west of 5W, and the cSEC is only observed west of the Greenwich Meridian.

Several of the equatorial PALACE floats experienced large meridional displacements ( $5^\circ$  or more) relative to their launch position, whereas none of the 6S PALACE floats experienced northward displacements of more than  $4^\circ$  throughout their mission (Fig. 3). This difference is due to the large impact of the surface flow on the trajectories of the equatorial PALACE floats (Fig. 8). A comparison of the meridional displacement due to the submerged drift reveals considerable similarities. Both north- and southward submerged displacements are visible in the 6S and the equatorial trajectories. It is noted that the net northward submerged displacements in the interior are always smaller than  $4^\circ$ . This lack of significant northward interior flow is in general agreement with results derived from SOFAR, MARVOR and RAFOS trajectories (Richardson and Schmitz, 1993; Ollitrault *et al.*, 1995; Boebel *et al.*, 1999a,b).

The schematic by Stramma and Schott (1999) shows a link between the cSEC and the NBUC via a southward loop near the western boundary (Fig. 1). PALACE 11 went through the southward limb of the loop (with an eddy-like motion), but it turned east at 12S instead of entering the boundary regime (Fig. 11d). This eastward motion is solely due to the submerged flow, as the surface flow is westward. Two RAFOS trajectories showed a similar behavior in the southward limb of the loop (Boebel *et al.*, 1999b). They ended their mission before showing signs of entering the NBUC or drifting toward the east. More observations are necessary to capture the proposed link between the cSEC and the NBUC with Lagrangian observations. PALACE 9 drifts westward in the cSEC until it is captured by the NBUC. Most of the zonal displacement (72%) and all of the meridional displacement is due to the submerged drift as PALACE 9 makes its way from 27W to 31W. Between 31W and 32W PALACE 9 stalls for about 2 months due to opposing flow at the surface and at depth. During this period the instrument might well have been just north of the cSEC. On the way from 32W to 34W the zonal submerged drift amounts to 57% of the total drift. These observations can be interpreted as a sign for a northward deflection of the cSEC near the western boundary. Such a pathway is not shown in Figure 1. It is not clear if the cSEC bifurcates, or if it turns south at some times and north at other times.

A broad northward flow parallel to the eastern boundary is observed in the LADCP and the PALACE float data (Figs. 7 and 11c). The mean submerged velocity from PALACE 14 is positive for 11 months. PALACE 19 also has a northward mean velocity over a period of more than 8 months. This northward flow is in general agreement with the similarity of the eastern AAIW at 6S and the equatorial AAIW (Fig. 5), even though the two PALACE floats did not reach the equator. These observations contradict the southward flow shown in Figure 1 (Stramma and Schott, 1999). Also, this northward flow and the westward mean flow (Fig. 9) east of the Mid-Atlantic Ridge do not support the hypothesis of a cyclonic

gyre in the eastern basin (Fig. 1). This hypothesis is largely based on the differences in the water properties of the eastern and the western basin (Warner and Weiss, 1992; Reid, 1989). The differences of the water mass characteristics (Figs. 5 and 6) between the two flow regimes east and west of 5W at 6S might be due to a closed-off cyclonic gyre, but this is not a necessary condition.

An analysis of the temporal variability of the flow south of the equator reveals the following: The SECC shows a preference for the latitude band between 7.5S and 5.5S and the cSEC is mostly north of 5.5S (Fig. 12). Stramma and Schott (1999) showed the SECC at 8S and the cSEC at 6S (Fig. 16). Results from earlier surveys (Fig. 2b) support the recent observations. It seems possible that both the cSEC and the SECC are frequently about 2° north of the latitude shown in Figure 1. The temporal variability visible in Figure 2b is consistent with the PALACE float data, which show signs of mesoscale and longer-period variabilities in individual trajectories (Fig. 11c and d). The time series of the zonal velocity in the region bounded by 6.5S to 5.5S, 15W to 5W (Fig. 14) indicates that the longer-period variability might be interpreted as a seasonal signal. However, there also seems to be a 2-month shift in the time of the current reversals between 1998 and 1999.

Before proceeding to the temporal variability of the EIC the vertical current structure on the equator, which is highly variable, will be discussed. For example, Schott *et al.* (1998) reported the vertical extent of predominantly westward flow at 35W as follows: 250 dbar to more than 1000 dbar in October 1990, 250 to 700 dbar in June 1991, 500 dbar to more than 1000 dbar in October 1992, and 200 to 850 dbar in March 1994. Three of their sections show two cores of maximum westward velocity, which are separated by a layer with weak westward or eastward velocities. Single velocity profiles on the equator obtained at different times also show alternating eastward and westward currents that can be between 100 and 800 m thick (Ponte *et al.*, 1990; Böning and Schott, 1993; Gouriou *et al.*, 1999). The equatorial LADCP section presented herein shows two cores of westward velocity between 100 and 1200 m to the west of 25W (Fig. 13). The upper core extends from 150 to 350 m at its maximum (at 35°W), and the lower core extends from about 500 to 1100 m in the western basin. In this paper the lower core is defined as the EIC, since its depth range agrees better with earlier observations and since it exists continuously across the whole basin.

Earlier observations suggested a seasonal cycle of the EIC. Based on Lagrangian data obtained in the AAIW layer the EIC was reported to exist from August to December and also sometimes in January through March while the current was not present from April until July (see Boebel *et al.*, 1999b for an overview). The seasonal reversal of the EIC was reproduced in an eddy-resolving, primitive equation model forced at the sea surface by seasonally varying surface wind stress (Böning and Schott, 1993). At the depth of the equatorial PALACE floats (900 to 1100 dbar), the mean simulated flow was weakly westward in October through December (about  $1 \text{ cm s}^{-1}$ ). In April through June a stronger mean eastward flow was found at the same depth (about  $5 \text{ cm s}^{-1}$ ). The direction of the simulated flow agrees well with the recent observations (Fig. 10a), but its velocity is

significantly smaller than the PALACE float velocities. The ensemble mean from all PALACE floats in the EIC is  $13 \text{ cm s}^{-1}$ .

The LADCP observations show westward flow between 600 m and more than 1000 m during the deployment week of 18 to 25 July 1997 (Fig. 13). In the 900 to 1000 m depth range this flow continues until the end of November 1997 within  $1^\circ$  of the equator. At this time PALACE 13 turns around at  $0.5S$  (Fig. 11b). After the reversal, PALACE 13 drifted northeastward and finally eastward near  $1^\circ N$  until the end of January 1998. No other PALACE float was within  $1^\circ$  of the equator during this time. The equatorial currents usually extend to at least  $\pm 1^\circ$  latitude; therefore, it seems likely that the EIC reversed at the end of November 1997. With the available data, however, it is not possible to determine whether or not the reversal is due to a change of the vertical extent of the EIC.

Boebel *et al.* (1999b) demonstrated that the termination of the westward EIC can occur at different times of the year. The recent data show that the onset of the westward EIC might vary as well. In 1997 the westward flow is observed two weeks earlier than previously thought. Under the assumption that these data are representative for the reversal of the EIC over its whole vertical extent, the results indicate that the EIC season is shifted to a slightly earlier time in 1997. Thus, it seems likely that the EIC season varies on interannual time scales, but more measurements are needed to resolve the influence of the observation depth on the results.

The PALACE float data from September 1997 to March 1998 suggest that the NICC velocity and latitude might depend on the longitude (Figs. 11a and b, and Table 1). The transition from higher to lower velocities occurs near  $28W$ , near the Mid-Atlantic Ridge. Results from a SOFAR trajectory presented by Richardson and Schmitz (1993) support this observation. The SOFAR float drifted eastward between  $2N$  and  $3N$  at  $800 \text{ m}$ . From  $27W$  on it drifted more slowly to  $12W$ . During this second period it was mostly at or south of  $2N$ . The change of the drift latitude at  $27W$  indicates that the NICC itself was farther south than during the drift west of  $27W$ . A second SOFAR float revealed a similar pattern. It drifted eastward between  $2N$  and  $3N$  at  $800 \text{ m}$  and turned south at  $30W$  to about  $1N$ . The eastward drift at this latitude continued to  $23W$ . Both the two SOFAR trajectories of Richardson and Schmitz (1993) and the five PALACE trajectories of the present study indicate that the NICC might be closer to the equator in the eastern basin than in the western basin. Reid (1994) presented a map of adjusted steric height at  $800 \text{ dbar}$  which supports the present observation of an eastward weakening of NICC, but the largest change in his map occurs near  $20W$  instead of near  $28W$ . A longitudinal dependence of the NICC latitude cannot be discerned in the Reid (1994) map.

Hydrographic observations have shown that the salinity front associated with the northern edge of the NICC can be anywhere between  $1N$  and  $3N$  (Suga and Talley, 1995). This range is valid for both the eastern and western basins. Therefore, the hydrographic data favor a scenario in which the NICC can undulate over the same latitude range in both basins, consistent with results based on several ADCP sections along  $44W$  and  $35W$ . At both longitudes the NICC was typically located between  $2N$  and  $3N$ , but during one survey

(in June 1991) the NICC core was between 1N and 2N at both longitudes (Schott *et al.*, 1998). The present Lagrangian observations and those obtained by Richardson and Schmitz (1993) indicate a longitudinal dependence of the NICC location, whereas the hydrographic and ADCP surveys are in favor of a time dependence of the NICC location. Most likely both the time and the longitude dependence prescribe the meridional position of the NICC. It remains to be seen if the east/west difference in the NICC location indicated by the Lagrangian observations is due to a sampling problem.

Model results by Böning and Schott (1993) indicate that the seasonal reversal of the EIC might coincide with a reversal of the NICC and the SICC. They presented two sections at 30W for the 400 to 3000 m depth range: In October to December the eastward NICC is visible between 2N and 5N below 1000 m, and the westward EIC extends from 900 m downward. During April to June the equatorial flow is eastward below 700 m, and the flow in 2N to 4N heads west throughout the water column. The time series of the observed zonal velocities in the band 1N to 3N seems to indicate a temporal variability of the current strength, with high velocities before March 1998 and low velocities after March 1998 (Fig. 10b). However, this signal is probably due to the poor sampling of the latitude band after March 1998. From April 1998 to January 1999 all data in this latitude range are between 20W and 25W, and the velocity does not reveal a seasonal signal. It is noted that this region does not seem to be representative for the NICC at other longitudes. The velocities between 20W and 25W differ significantly from those east or west of 20W to 25W during the period September 1997 to March 1998. Reversals of the submerged drift in individual trajectories (Fig. 11a and b) can also help to clarify if a current reverses. It is noted that they usually coincide with meridional displacements of  $1^\circ$  or more. The only exception is the trajectory of PALACE 13, which shows frequent reversals without significant meridional displacements. But these reversals do not occur on seasonal time scales. Velocity sections by Schott *et al.* (1998) are also in favor of a permanently existing NICC. It is concluded that the observations to date do not reveal a seasonal reversal of the NICC, but that there might be periods of weaker or reversed flow between 25W and 20W.

In terms of high frequency variability, Molinari *et al.* (1999) proposed that Rossby waves might trigger the reversals seen in the trajectories of the PALACE floats launched at the equator (Figs. 11a and b). Wave-like patterns can be found in some of the equatorial trajectories. The meridional velocity of trajectories 3 and 13 reveals a period of 30 days to 45 days (Fig. 15). SOFAR and RAFOS trajectories also show meandering on the equator at similar periods as the PALACE float trajectories (Richardson and Schmitz, 1993; Boebel *et al.*, 1999b), but they do not experience the northward transitions found in the PALACE float trajectories. The northward transitions of the PALACE floats hence appear to be caused by the cyclic surfacing, rather than by a permanent northward displacement of a water parcel.

In a modeling study, Böning and Schott (1993) also find high frequency variability in the deep meridional velocity on the equator. The variability at 1875 m is characterized by wavelengths of about 1000 km and periods of about 45 days (similar to the period derived

from the PALACE float data). The phase and group velocity of these waves are consistent with Rossby-gravity waves. The westward increase of the wave amplitude in PALACE 13 indicates that the Mid-Atlantic Ridge might have an impact on the waves. Another possibility is that vertically propagating energy from the tropical instability waves at the surface can induce variability at these periods just north of the equator (Cox, 1980). The region of maximum amplitudes in the meandering trajectories (central Atlantic, Fig. 11a and b) and the time of the year (early summer through late fall) agree with the observations of tropical instability waves (e.g. Weisberg and Weingartner, 1988).

*Acknowledgments.* We wish to acknowledge the outstanding performance of the RV *Seward Johnson* crew during the deployment cruise. We want to thank Molly O. Baringer who was the chief scientist of the cruise, Dave Bitterman for preparing the PALACE floats and processing software, Christiane I. Fleurant for calibration of the CTD data and Ryan Smith for processing of the LADCP data. We are also grateful for the software to estimate tidal currents which was provided by Eric Firing and colleagues. This work is partially sponsored by NOAA's Office of Global Programs. This research was carried out in part under the auspices of the Cooperative Institute for Marine and Atmospheric Studies (CIMAS) a joint institute of the University of Miami and the National Oceanic and Atmospheric Administration (NOAA), cooperative agreement #NA67RJ0149.

## APPENDIX

### Extrapolation of surface drift

Each time a PALACE float goes through its surface cycle a time lag between the actual first (last) surface time and the estimation of the first (last) surface position by ARGOS occurs. A best estimate for the surface drift has to be derived to reduce the error in the submerged drift and for the location of the profile. Davis *et al.* (1991) developed a method for the estimation of the surface drift based on cokriging. Essentially one is looking for a solution of

$$x_c = \sum_{i=1}^N w_1(i) * x(i) + \sum_{i=1}^N w_2(i) * y(i)$$

$$y_c = \sum_{i=1}^N w_1(i) * y(i) + \sum_{i=1}^N w_2(i) * x(i).$$

Here  $x$  and  $y$  are the observed longitude and latitude,  $w_1$  and  $w_2$  are weights,  $x_c$  and  $y_c$  are the estimated longitude and latitude, and  $N$  is the number of observed positions. One must solve

$$C * \mathbf{w} = \mathbf{z}$$

where  $C$  is the matrix

$$\begin{pmatrix} c(x_1, x_1) - e_1 & \cdots & c(x_1, x_N) & c(x_1, y_1) & \cdots & c(x_1, y_N) & 1 & 0 \\ \vdots & & \vdots & \vdots & & \vdots & \vdots & \vdots \\ c(x_N, x_1) & \cdots & c(x_N, x_N) - e_N & c(x_N, y_1) & \cdots & c(x_N, y_N) & 1 & 0 \\ c(y_1, x_1) & \cdots & c(y_1, x_N) & c(y_1, y_1) - e_1 & \cdots & c(y_1, y_N) & 0 & 1 \\ \vdots & & \vdots & \vdots & & \vdots & \vdots & \vdots \\ c(y_N, x_1) & \cdots & c(y_N, x_N) & c(y_N, y_1) & \cdots & c(y_N, y_N) - e_N & 0 & 1 \\ 1 & \cdots & 1 & 0 & \cdots & 0 & 0 & 0 \\ 0 & \cdots & 0 & 1 & \cdots & 1 & 0 & 0 \end{pmatrix}$$

and

$$\mathbf{w} = [w_1(1) \dots w_1(N) w_2(1) \dots w_2(N) - \lambda_1 - \lambda_2]^T$$

$$\mathbf{z} = [c(x_1, x_c) \dots c(x_N, x_c) c(y_1, y_c) \dots c(y_N, y_c)]^T$$

The vector  $\mathbf{e} = [e_1 \dots e_N]$  contains the measurement errors and  $\lambda_1$  and  $\lambda_2$  are the Lagrangian multipliers. The elements  $c$  of the matrix  $C$  and the vector  $\mathbf{z}$  are either the covariances or the dissimilarities, depending on the chosen approach for solving the equation system.

The equation system can be solved with two approaches. One is to estimate the covariances and find a covariance model that fits the data. The other is to estimate the dissimilarities (the variogram) and again find a structure function that fits the data. The latter approach will be used here. The coefficients for the structure function can be estimated from data in three different ways:

- 1) Estimate the coefficients in certain regions of the ocean (Hansen and Poulain, 1996).
- 2) Calculate the coefficients for each track individually.
- 3) Estimate the coefficients based on a big data set of daily trajectories and use the correlation between the coefficients and the mean surface drift velocity to choose the coefficients.

The first possibility was not used since the definition of the regions poses problems. These are mainly that (a) certain regions can have a high variability which would increase the error of using one fixed set of coefficients, and that (b) the usage of rectangular boxes in the boundary currents is not a good approach.

Surface drifter trajectories were used to identify the best of the methods 2 and 3 for the estimation of the structure function and its coefficients. Subsets of the trajectories were extrapolated to one data point before and after the time period used for the extrapolation (Fig. 17, upper panel). Several different structure functions were studied and it was found that the function  $f(t) = \alpha(t/T)^2 \exp(-t/T)$  yielded the best results. This structure function is different from that used by Davis *et al.* (1991). The variables are the time scale  $T$ , the time  $t$  and the structure function coefficient  $\alpha$ . The time scale and location errors have been

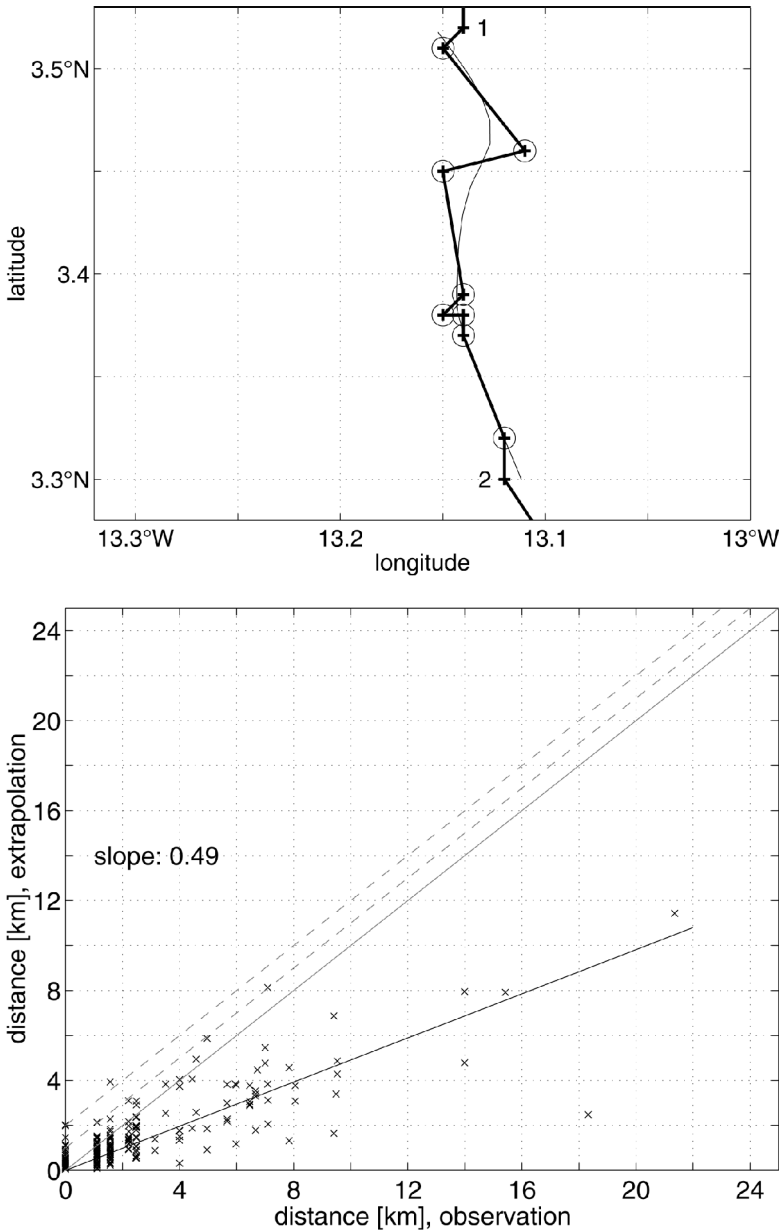


Figure 17. Results from the extrapolation. Upper panel: Example for one trajectory segment. The thick line marked with plusses is the observed trajectory. The circles indicate the positions used for the extrapolation. The thin line is the extrapolated trajectory corresponding to the drift from 1 to 2. Lower panel: Example for the quality of extrapolation (based on 100 trajectory segments). The crosses indicate the distances from the observed locations. The solid curve is a linear fit to the crosses with a slope of 0.49. The three parallel lines have a slope of one (solid indicates identical distances, dashed indicates 1 km or 2 km deviation).

varied for the two methods (2) and (3). Method (2) lead to the smallest extrapolation errors, with a time scale ( $T$ ) of 3 days and location errors of 2000 m, 1000 m, 500 m and 333 m. These location errors are based on the location classes given by ARGOS.

In the example presented in Figure 17 the extrapolation reduces the error of the surface positions by 51% on average. In about 74% of the cases the location error has been reduced whereas only 25% of the estimated distances from the actual surface position are slightly enlarged. In only 4% (1%) of the cases the distance is more than 1 km (2 km) larger than in reality. When looking at this result one should remember that the ARGOS error can exceed 1 km. From this comparison one can conclude that the usually achieved improvement of the location exceeds the loss of precision in these few cases.

#### REFERENCES

- Boebel, O., R. E. Davis, M. Ollitrault, R. G. Peterson, P. L. Richardson, C. Schmid and W. Zenk. 1999a. Direct observations of the western South Atlantic intermediate depth circulation. *Geophys. Res. Lett.*, *26*, 3329–3332.
- Boebel, O., C. Schmid and W. Zenk. 1999b. Kinematic elements of Antarctic Intermediate Water in the western South Atlantic, *in* New Views of the Atlantic, W. Zenk, R. G. Peterson and J. R. E. Lutjeharms, eds., *Deep-Sea Res. II*, *46*, 355–392.
- Böning, C. and F. A. Schott. 1993. Deep currents and the eastward salinity tongue in the equatorial Atlantic: Results from an eddy-resolving, primitive equation model. *J. Geophys. Res.*, *98*, 6991–6999.
- Chepurin, G. and J. A. Carton. 1997. The hydrography and circulation of the upper 1200 meters in the tropical North Atlantic during 1982–91. *J. Mar. Res.*, *55*, 633–670.
- Cox, M. D. 1980. Generation and propagation of 30-day waves in a numerical model of the Pacific. *J. Phys. Oceanogr.*, *10*, 1168–1186.
- Davis, R. E., D. C. Webb, L. A. Regier and J. Dufour. 1991. The Autonomous Lagrangian Current Explorer. *J. Atmos. Oc. Technol.*, *9*, 264–285.
- Dushaw, B. D., G. D. Egbert, P. F. Worcester, B. D. Cornuelle, B. M. Howe and K. Metzger. 1997. A TOPEX/POSEIDON global tidal model (TPXO.2) and barotropic tidal currents determined from long-range acoustic transmissions. *Prog. Oceanogr.*, *40*, 337–367.
- Egbert, G. D., A. F. Bennet and M. G. G. Foreman. 1994. TOPEX/POSEIDON tides estimated using a global inverse model. *J. Geophys. Res.*, *99*, 24,821–24,852.
- Fleurant, C. I., R. L. Molinari, R. H. Smith, M. O. Baringer and W. D. Wilson. 1999. CTD, LADCP, XBT, and PALACE float measurements collected on an Atlantic Ocean Circulation Experiment (ACCE) cruise along 6°N, 6°S, and the equator during June–August 1997. NOAA/AOML Miami.
- Gouriou, Y., B. Bourlès, H. Mercier and R. Chuchla. 1999. Deep jets in the equatorial Atlantic Ocean. *J. Geophys. Res.*, *104*, 21,217–21,226.
- Hansen, D. V. and P.-M. Poulain. 1996. Quality control and interpolations of WOCE-TOGA drifter data. *J. Atmos. Oc. Technol.*, *13*, 900–909.
- Molinari, R. L. 1982. Observations of eastward currents in the Tropical South Atlantic Ocean: 1978–1980. *J. Geophys. Res.*, *87*, 9707–9714.
- Molinari, R. L., S. L. Garzoli and R. W. Schmitt. 1999. Equatorial Currents at 1000 m in the Atlantic Ocean. *Geophys. Res. Lett.*, *26*, 361–363.
- Ollitrault, M., Y. Auffret, N. Cortès, C. Hémon, P. Jégou, S. L. Reste, G. Loaëc and J.-P. Rannou. 1995. The SAMBA Experiment. Volume 1, SAMBA I, Lagrangian and CTD Data. February 1994–August 1995. *Repères océan* No. 12, 622 pp.
- Ponte, R. M., J. Luyten and P. L. Richardson. 1990. Equatorial deep jets in the Atlantic Ocean. *Deep-Sea Res.*, *37*, 711–713.



- Reid, J. L. 1989. On the total geostrophic circulation of the South Atlantic Ocean: Flow patterns, tracers and transports. *Prog. Oceanogr.*, *23*, 149–244.
- 1994. On the total geostrophic circulation of the North Atlantic Ocean: Flow patterns, tracers and transports. *Prog. Oceanogr.*, *33*, 1–92.
- Richardson, P. L. and W. J. Schmitz. 1993. Deep cross-equatorial flow in the Atlantic measured with SOFAR floats. *J. Geophys. Res.*, *98*, 8371–8387.
- Schott, F. A., J. Fischer and L. Stramma. 1998. Transports and pathways of the upper-layer circulation in the western Tropical Atlantic. *J. Phys. Oceanogr.*, *28*, 1904–1928.
- Stramma, L. 1991. Geostrophic transport of the South Equatorial Current in the Atlantic. *J. Mar. Res.*, *49*, 281–294.
- Stramma, L. and F. A. Schott. 1999. The mean flow field of the tropical Atlantic Ocean, *in* *New Views of the Atlantic*, W. Zenk, R. G. Peterson and J. R. E. Lutjeharms, eds., *Deep-Sea Res. II*, *46*, 279–303.
- Suga, T. and L. D. Talley. 1995. Antarctic Intermediate Water circulation in the tropical and subtropical South Atlantic. *J. Geophys. Res.*, *100*, 13,441–13,453.
- Tsuchiya, M., L. D. Talley and M. S. McCartney. 1994. Water-mass distributions in the western South Atlantic; A section from South Georgia Island (54S) northward across the equator. *J. Mar. Res.*, *52*, 55–81.
- Warner, M. J. and R. F. Weiss. 1992. Chlorofluoromethanes in South Atlantic Antarctic Intermediate Water. *Deep-Sea Res.*, *39*, 2053–2075.
- Weisberg, R. H. and T. J. Weingartner. 1988. Instability waves in the equatorial Atlantic Ocean. *J. Phys. Oceanogr.*, *18*, 1641–1657.